A glial cell derived pathway directs regenerating optic nerve axons toward the optic chiasm

Running Title: Glia direct regenerating RGC axons

Beth M. Harvey[1*], Melissa Baxter[1], Alexis M. Garcia[1] and Michael Granato[1]

Department of Cell and Developmental Biology, Perelman School of Medicine, University of Pennsylvania, Philadelphia, Pennsylvania 19104

* Corresponding author

email: bharvey@pennmedicine.upenn.edu

Key words: lh3, collagen18a1, RGC, optic nerve regeneration, axon guidance, zebrafish

Abstract

After optic nerve injury, several retinal ganglion cell (RGC) intrinsic signaling pathways have been shown to enhance RGC survival and RGC axonal growth. In contrast, few extrinsic cues have been identified that guide regenerating RGC axons toward and across the optic chiasm. Here, we use live-cell imaging in larval zebrafish to show that regrowing RGC axons initiate growth toward the midline and extend along a trajectory similar to their original projection. From a candidate genetic screen, we identify the glycosyltransferase Lh3 (also referred to as Plod3) to be required to direct regrowing RGC axons toward the midline during active regeneration. Moreover, we show that transgenic *lh3* expression in *sox10*+ presumptive *olig2*+ oligodendrocytes located near the optic chiasm restores directed axonal growth in *lh3* mutants. Finally, we find that mutants in *collagen 18a1 (col18a1),* a putative Lh3 substrate, display RGC axonal misguidance phenotypes similar to *lh3* mutants, suggesting that *lh3* may act through *col18a1* during regeneration. Combined, these data identify *lh3* as part of a glial derived molecular pathway critical for guiding *in vivo* regenerating RGC axons toward and across the optic chiasm.

33 **Introduction**

34 As a component of the central nervous system, retinal ganglion cell (RGC) axons within
35 the mammalian optic nerve display a poor regenerative capacity. Multiple factors contribute to the
36 minimal regeneration in mammals, including massive injury-induced RGC death and overall
37 limited axonal regrowth (Villegas-Pérez *et al.*, 1993; Berkelaar *et al.*, 1994; Goldberg *et al.*, 2002).
38 Several studies have identified a number of RGC intrinsic signaling pathways that enhance RGC
39 survival and increase long range axonal growth after injury. For example, deletion of the
40 transcriptional repressor KLF4 in RGCs increases axonal regrowth (Moore *et al.*, 2009). Similarly,
41 activation of inflammatory responses within the retina through injection of Zymosan and cAMP
42 enhances cell survival and axonal regrowth (Leon *et al.*, 2000; Goldberg *et al.*, 2002; Yin *et al.*,
43 2009). Moreover, deleting intrinsic factors in RGCs such as PTEN and TSC1, which function as
44 negative regulators of the mTOR pathway, improves both RGC cell survival and axonal growth
45 (Park *et al.*, 2008; Smith *et al.*, 2009; Norsworthy *et al.*, 2017). However, enhancing RGC axonal
46 growth by manipulating RGC intrinsic programs frequently results in axonal misguidance as axons
47 project inappropriately from the optic tract before and at the optic chiasm during the initial stages
48 of regeneration (Kurimoto *et al.*, 2010; Luo *et al.*, 2013; Vincent Pernet *et al.*, 2013; V. Pernet *et*
49 *al.*, 2013; Berry, Ahmed and Logan, 2019). This demonstrates a need to identify molecular and
50 cellular mechanisms that guide RGC axons as they regrow toward and across the optic chiasm
51 during regeneration.

52 Following a Central Nervous System (CNS) injury in mammals, many non-neuronal cells
53 create an extracellular environment that is largely inhibitory to axonal regrowth. The cellular and
54 molecular barriers that form within a lesion site have long been attributed to an influx of
55 inflammatory cells and the upregulation of inhibitory molecules not conducive for robust
56 regeneration (Yiu and He, 2006; Fitch and Silver, 2008). Additional studies in mice have since
57 revealed roles for microglia and oligodendrocytes in functional recovery and remyelination from

58 CNS injury (Wang *et al.*, 2020; Mendonça *et al.*, 2021; Brennan *et al.*, 2022). Yet due to the
59 dominance of factors inhibiting axonal regrowth, the cellular and molecular mechanisms that guide
60 regrowing RGC axons following axonal injury are largely unknown. Recently, spontaneous CNS
61 regeneration has been described in two mammalian species, the naked mole rat and the spiny
62 mouse, demonstrating that pro-regenerative environments that support robust CNS regeneration
63 are not unique to the CNS of non-mammalian vertebrates (Park *et al.*, 2017; Nogueira-Rodrigues
64 *et al.*, 2022). Therefore, model organisms that exhibit spontaneous robust CNS axonal
65 regeneration, without an overwhelmingly inhibitory extracellular environment, provide unique
66 opportunities to identify mechanisms that promote CNS regeneration.

67 We recently developed a rapid and robust optic nerve transection assay in larval zebrafish
68 to take full advantage of its regenerative capabilities and optical transparency to study functional
69 optic nerve regeneration *in vivo* (Harvey, Baxter and Granato, 2019, 2023). At just 5 days post
70 fertilization (dpf), larval zebrafish already possess a functional visual system driving several
71 visually guided behaviors, such as prey capture (Brockerhoff *et al.*, 1995; Easter and Nicola, 1996;
72 Gahtan, Tanger and Baier, 2005). Following complete transections of the RGC axons in 5 dpf
73 larvae, we observe axonal degeneration, subsequent initiation of regrowth and reinnervation of
74 the optic tecta by 72 hours post transection (hpt) (Harvey, Baxter and Granato, 2019). We have
75 also shown that RGC axonal regeneration in larval zebrafish occurs independent of RGC death
76 or neurogenesis, and that visual function is restored by 8 days post transection (Harvey, Baxter
77 and Granato, 2019). Using this optic nerve transection assay, we performed a candidate genetic
78 screen and identify Lh3, a collagen-modifying glycosyltransferase whose gene name is referred
79 to as *lh3* or also *plod3*, to be critical for directing axonal regrowth toward the optic chiasm during
80 optic nerve regeneration. We show that following optic nerve transection, *lh3* expression is
81 upregulated near the site of axonal injury and that Lh3 functions during the time when active
82 regeneration occurs, specifically during the early stages of regeneration as RGC axons are

83 growing toward the midline. We also show that Lh3 expression in oligodendrocytes is required to
84 direct early regrowing RGC axons across the midline along their original path. Furthermore, we
85 show that mutants in *collagen 18a1 (col18a1),* a putative Lh3 substrate, display RGC axonal
86 misguidance phenotypes similar to *lh3* mutants, indicating at a glial-derived molecular pathway in
87 which Lh3 acts through Collagen18a1 to direct RGC axons. Combined, our results demonstrate
88 a critical pro-regenerative *in vivo* role for oligodendrocytes during early optic nerve regeneration
89 to direct axon regrowth toward and across the midline.
90

91 ## Results

92 **Lh3 is required for growth across midline during regeneration**

93 To identify molecular mechanisms that guide regrowing RGC axons across the optic
94 chiasm during optic nerve regeneration, we performed a candidate genetic screen consisting of
95 35 genes that are expressed in the visual system or have known functions in axon growth and
96 guidance. Specifically, we used a sharpened tungsten needle to transect the optic nerves of
97 genetic mutants and their siblings at 5 dpf and assessed at 72 hpt whether RGC axons had
98 regrown across the optic chiasm to reinnervate the optic tectum. One of the top hits from this
99 screen was the gene *lh3*, which encodes a multidomain glycosyltransferase that post-
100 translationally modifies collagen proteins (Heikkinen *et al.*, 2000; C. Wang *et al.*, 2002). RGC axon
101 projections in *lh3* mutants cross the midline and project to the optic tecta in a manner
102 indistinguishable to their siblings (Zeller *et al.*, 2002). However, we took advantage of a previously
103 validated transgene *Tg(hsp70:lh3-myc)*, which expresses a Myc-tagged Lh3 under the control of
104 the *hsp70* heat-shock-activated promoter (Isaacman-Beck *et al.*, 2015) to rescue various
105 morphological deficits that would affect the survivability of the larvae for the duration of the
106 regeneration experiments (Zeller and Granato, 1999; Taler *et al.*, 2019) (Fig. 1A). At 5 dpf,
107 uninjured RGC axons in both *lh3* siblings and mutants exit the eye and project across the optic

108 chiasm to terminate in the optic tecta (Fig. 1B-E). Following optic nerve transection, axons in *lh3*
109 siblings grow across the midline and reinnervate the optic tecta (Fig. 1F,H,J,L). In contrast,
110 transected optic nerve axons in *lh3* mutants fail to cross the midline and instead project along
111 aberrant trajectories, often along anterior and posterior paths or also dorsally or ventrally (Fig
112 1G,I,K,L, magenta arrowheads). These results reflect a functional role for Lh3 during optic nerve
113 regeneration in directing RGC axons towards and across the midline at the optic chiasm.

114 ***Lh3* expression is upregulated in the optic chiasm during regeneration**

115 We next asked whether Lh3 is required during the process of optic nerve regeneration. For
116 this, we took advantage of the conditional *Tg(hsp70:lh3-myc)* transgene (Isaacman-Beck *et al.*,
117 2015). We induced Lh3 expression in 5 dpf larvae 4-5 hours prior to performing the optic nerve
118 transections, and then assessed axonal regrowth across the optic chiasm and reinnervation of
119 the optic tecta at 72 hpt (Fig. 2A). RGC axons in *lh3* siblings that did or did not receive a heat
120 shock regrew across the midline and innervated the optic tecta (Fig. 2B,D,F). In contrast, *lh3*
121 mutants without a heat shock display aberrant axonal growth, while heat shock induced Lh3
122 expression in *lh3* mutants restores optic nerve axonal regrowth across the midline (Fig. 2C,E-F).
123 These data demonstrate that Lh3 acts during the process of optic nerve regeneration.

124 We then sought to determine in which cell-type Lh3 was expressed during optic nerve
125 regeneration. We used *in situ* hybridization chain reaction to detect *lh3* mRNA expression prior to
126 and after optic nerve transections. Prior to transections, we failed to detect *lh3* mRNA expression
127 in retinas nor in the region of the optic chiasm (Fig. 2G-I; n = 17 larvae). Similarly, after transection,
128 we failed to detect *lh3* mRNA expression in RGC neurons in the retina (Fig. 2G-H; n = 41 larvae).
129 In contrast, we detected upregulated *lh3* mRNA expression around the transected proximal stump
130 of RGC axons and near the midline during early regeneration between 2 and 6 hpt (Fig. 2G,I; n =
131 30/41 larvae), demonstrating that *lh3* mRNA is upregulated following optic nerve transection in
132 the region of the optic chiasm.

133 **Lh3 directs regrowing RGC axonal growth toward their original trajectory**

134 Following optic nerve transections in wild-type larvae, we have previously observed new
135 RGC axons emerging from the proximal stump of transected optic nerves by 24 hpt and exhibit
136 robust growth across the optic chiasm by 48 hpt (Harvey, Baxter and Granato, 2019). To determine
137 whether Lh3 continuously directs regenerating RGC axons once they emerge from the optic nerve
138 stump, we used live cell imaging and examined the dynamics of regenerating RGC axons as they
139 approach and cross the optic chiasm, which has not previously been reported. For simplicity, we
140 removed one eye from 4 dpf larvae to only visualize the regrowth from a single retina per larva,
141 and then performed transections to timelapse *lh3* siblings and mutants (Fig 3A, S1). Following
142 transections on 5 dpf *lh3* sibling and mutant larvae, we observe that the portion of axons distal to
143 the transection site undergoes Wallerian degeneration, as has been observed for other nerves in
144 zebrafish (Fig. 3B-D,G-I, Supplementary Movies 1 and 2, brackets) (Waller, 1851; Martin *et al.*,
145 2010; Rosenberg *et al.*, 2012; Bremer *et al.*, 2019). In *lh3* siblings, some axons emerge from the
146 proximal stump of RGC axons in a range of directions, often extending and retracting rapidly (Fig.
147 3B-C, Supplementary Movie 1). By 16 hpt, we observe that a small group of axon fascicles grows
148 toward the midline and rapidly extends across the midline (Fig. 3D-E, Supplementary Movie 1,
149 white arrowheads). Over the next few hours, additional fascicles of axons are observed following
150 the growth of the axons that have crossed the midline (Fig. 3F, Supplementary Movie 1) revealing
151 *in vivo* axonal dynamics during the early stages of optic nerve regeneration. Axons in *lh3* mutants
152 emerge at similar timepoints to *lh3* siblings from the proximal stump (Fig 3G-H, Supplementary
153 Movie 2). However, unlike the *lh3* siblings, axonal growth does not persist across the midline and
154 axons often grow anteriorly and posteriorly or dorsally and ventrally around the eye (Fig. 3I-K,
155 Supplementary Movie 2, magenta arrowheads), strongly suggesting that during the early process
156 of optic nerve regeneration, Lh3 directs the initial regrowth of RGC axons toward the midline.

157 We next sought to identify the mechanisms by which Lh3 directs regrowing RGC axons
158 toward and across the optic chiasm. We first asked whether Lh3 is critical for the initiation of
159 axonal growth extending from the proximal stump of transected RGC axons, and consequently
160 whether optic nerve regrowth was delayed in *lh3* mutants. We found no significant difference in
161 the timing of initiation of axonal regrowth post transection (Fig 4A-B). To further define the
162 trajectories that RGC axons take as they grow across the optic chiasm, we measured the angle
163 between distinct axon fascicles and the original projection path before transection (Fig 4C; see
164 Methods for more details). In optic nerves in *lh3* siblings and mutants that regrew across the
165 midline, we observe that while some fascicles strayed from the pre-injury path, most fascicles
166 grow very close to their original projection path (Fig 4D; Supplemental Table 1). Nerves in *lh3*
167 siblings that did not grow toward the midline grew along a mostly single aberrant trajectory (Fig
168 4D; Supplemental Table 1). In contrast, in nerves that failed to cross the midline in *lh3* mutants,
169 we found that the aberrant paths of axon projections displayed a much greater range of angles
170 (Fig 4D; Supplemental Table 1). These data strongly suggest that *lh3* is required to direct RGC
171 axons along their regenerative path, which is very similar to their pre-transection path, towards
172 and across the optic chiasm.

173 **Glial expression of Lh3 restores RGC axonal growth across the midline**

174 Given that *lh3* mRNA expression is upregulated in area of the optic chiasm (Fig. 2I) and
175 that *lh3* is required *in vivo* to direct regenerating RGC axons along their original projection path
176 (Fig. 2F, 3, 4D), we hypothesized that the relevant cell type critical for *lh3* mediated optic nerve
177 regeneration would be located in the region of the optic chiasm. Transcriptomics studies in mice
178 have found *lh3* to be expressed most greatly in microglia (Zhang *et al.*, 2014). Moreover,
179 macrophages and microglia have been shown to clear debris from injured axons and can promote
180 axonal growth and remyelination during CNS regeneration (Rosenberg *et al.*, 2012; Wang *et al.*,
181 2020; Brennan *et al.*, 2022). Therefore, we first focused on macrophages and microglia as a

182 potential source of Lh3 activity during optic nerve regeneration. In untransected larvae, we
183 observe sporadic *mpeg*+ cells near the optic chiasm (Fig 5A). At 24 hpt, we observe a greater
184 concentration of *mpeg*+ cells surrounding the proximal stump of RGC axons and the new axonal
185 growth (Fig. 5A; n = 11 larvae). We next used a transgenic rescue approach to test whether
186 expression of *lh3* in macrophages/microglia is sufficient to restore axonal regrowth across the
187 optic chiasm in *lh3* mutants. We found that Lh3 expression from a *Tg(mpeg:lh3-myc)* transgene
188 fails to rescue the *lh3* mutant phenotype, where nerves in *lh3* mutants mostly display aberrant
189 growth similar to *lh3* mutants without the *Tg(mpeg:lh3-myc)* transgene (Fig 5D). Since RGC axons
190 regrow very closely to their original path, we next sought to examine oligodendrocytes associated
191 with the optic nerve (Brösamle and Halpern, 2002). Using both a *Tg(olig2:dsred)* transgenic line
192 labeling oligodendrocyte lineage cells (Fig 5B, n= 5 untransected larvae, n = 21 transected larvae)
193 as well as *in situ* hybridization chain reactions for *mbpa* mRNA in myelinating oligodendrocytes
194 (Fig 5C, n= 6 untransected larvae, n = 5 transected larvae), we observed oligodendrocytes in the
195 optic chiasm and associated with RGC axons before and after transection (Kucenas *et al.*, 2008;
196 Ackerman and Monk, 2016). We then tested whether expression of *lh3* in oligodendrocytes would
197 rescue axonal regrowth across the optic chiasm in *lh3* mutants. *Sox10*, like *olig2,* is a transcription
198 factor that mediates oligodendrocyte lineage specificity and is maintained in all oligodendrocyte
199 lineage cells (Bergles and Richardson, 2015; Ackerman and Monk, 2016). We find that *lh3*
200 expression from a *Tg(sox10:lh3-mkate)* transgene restores RGC regrowth across the midline in
201 otherwise mutant *lh3* larvae (Fig 5E). Furthermore, we detect *lh3* mRNA expression that overlaps
202 with transgenic labeling of oligodendrocyte cells, demonstrating that *lh3* is upregulated in
203 oligodendrocytes surrounding the proximal stump of transected RGC axons and along an axonal
204 projection path across the midline during optic nerve regeneration (Fig. 5F-G, Supplemental
205 Movie 3; n = 15/21). Altogether, these findings demonstrate that *lh3* expression in

206 oligodendrocytes near the proximal stump of transected RGC axons directs early regrowing RGC
207 axons toward the midline along their original path to reinnervate the optic tecta.

208 **Col18a1 is also critical for directing regenerating RGC axons**

209 We further sought to identify the relevant Lh3 substrate during optic nerve regeneration.
210 Given the well documented role of Lh3 in post-translationally modifying collagen proteins
211 (Heikkinen *et al.*, 2000; C. Wang *et al.*, 2002), we focused on collagen substrates. As part of our
212 initial candidate genetic screen, we examined *col4a5*, which is required for proper RGC axon
213 targeting of tectal layers and also functions to scaffold guidance cues during both the development
214 of the visual system and during motor nerve regeneration (Xiao and Baier, 2007; Xiao *et al.*, 2011;
215 Isaacman-Beck *et al.*, 2015; Murphy, Isaacman-Beck and Granato, 2022). We also tested *col7a1,*
216 which has been shown to be expressed in the eye (Wullink *et al.*, 2018). We ultimately found that
217 RGC axon regeneration toward and across the midline is unaffected in *col4a5* and *col7a1* mutants
218 (Fig. S2). We then examined *col18a1*, a collagen associated with Knobloch syndrome in humans
219 that is characterized by eye abnormalities (Fukai *et al.*, 2002; Suzuki *et al.*, 2002). Col18a1 has
220 several putative Lh3 sites within X-Lys-Gly- motifs and has been shown *in vitro* to bind to Lh3
221 (Risteli *et al.*, 2004; Salo and Myllyharju, 2021). First, we used *in situ* hybridization chain reaction
222 to detect *col18a1* mRNA expression and observe an upregulation of *col18a1* mRNA at 12 hpt in
223 the optic chiasm, similar to the expression pattern of *lh3* following optic nerve transection (Fig.
224 6A; n = 13/14 larvae). We also detect *col18a1* mRNA expression that overlaps with transgenic
225 labeling of oligodendrocyte cells, which demonstrates that *col18a1* is also upregulated in
226 oligodendrocytes surrounding the proximal stump of transected RGC axons and along axonal
227 projection path across the midline during optic nerve regeneration (Fig. 6B, Supplementary Movie
228 4). We then tested *col18a1* mutants in our optic nerve transection assay. Prior to transection, RGC
229 axonal projections were indistinguishable between *col18a1* siblings and mutants (Fig. 6C-F). In
230 contrast, at 72 hpt we observed regrowing RGC axons projecting away from the CNS midline,

231 similar to what we observe in *lh3* mutants where regenerating RGC axons grow along aberrant
232 paths (Fig 6G-K). This demonstrates that during regeneration *col18a1* is critical for directing
233 regenerating RGC axons toward the midline and suggests that glial-derived Lh3 acts, as least in
234 part, through Col18a1 during optic nerve regeneration.
235

236 ## Discussion

237 Regenerating axons often encounter multiple choice points along their paths that they must
238 navigate properly to robustly reinnervate their original targets. Previous studies have shown that
239 PTEN inactivation in RGC neurons strongly promotes RGC regrowth following an optic nerve
240 injury, but that these axons display axonal misguidance at the optic chiasm, proving the optic
241 chiasm to be one such choice point (Kurimoto *et al.*, 2010; Luo *et al.*, 2013; Vincent Pernet *et al.*,
242 2013; V. Pernet *et al.*, 2013; Berry, Ahmed and Logan, 2019). Here, we identify a mechanism
243 critical for guiding RGC axons toward and across the optic chiasm during optic nerve
244 regeneration. We find that *lh3* is required during regeneration to direct regenerating RGC axons
245 toward and across the midline. We find that following optic nerve transection, expression of *lh3*
246 and its presumptive substrate *col18a1* are upregulated in cells along the regenerative path near
247 the optic chiasm. Using live cell imaging, we demonstrate that *lh3* is required to direct regrowing
248 RGC axons along a regenerative trajectory very similar to their original path. Together, these
249 results provide compelling evidence for a RGC extrinsic molecular pathway that guides optic
250 axons during regeneration.

251 **Live cell imaging reveals axonal dynamics of early optic nerve regeneration**

252 To date, most optic nerve regeneration studies in adult rodents and fish monitor RGC
253 axonal regrowth with static time point analyses (Horder, 1971; Murray, 1976; V. Pernet *et al.*, 2013;
254 Yin and Benowitz, 2018). In contrast, peripheral nervous system regeneration, as well as spinal
255 cord regeneration have been visualized in live larval zebrafish using *in vivo* imaging studies (Bhatt

256 *et al.*, 2004; Rosenberg *et al.*, 2012; Ceci *et al.*, 2014; Lewis and Kucenas, 2014; Isaacman-Beck
257 *et al.*, 2015; Bremer *et al.*, 2019). To visualize RGC axonal dynamics during optic nerve
258 regeneration, we previously established an optic nerve transection assay in larval zebrafish
259 (Harvey, Baxter and Granato, 2019, 2023). Here, we perform live cell imaging of RGC axons
260 initiating regrowth and regenerating across the optic chiasm *in vivo*. These timelapses reveal two
261 intriguing insights into mechanisms that may mediate robust CNS regeneration in zebrafish. First,
262 we observe that axons distal to the transection site undergo Wallerian degeneration (Fig. 3B-D,G-
263 I, Movie S1 and Movie S2, brackets) (Waller, 1851). While a hallmark of the mammalian CNS is
264 a slower rate of axonal fragmentation following axonal injury, here we observe complete
265 degeneration of the distal axons by about 15 hpt (Vargas and Barres, 2007). While we did not
266 examine whether persistence of degenerating debris would repel axonal growth, we do observe
267 new axons reaching the midline around the same time axonal debris is cleared from that region
268 (Fig. 3D). Axonal debris and associated myelin proteins are known to inhibit axonal regeneration
269 (Vargas and Barres, 2007). But here, we find that Wallerian degeneration does not appear to be
270 delayed in *lh3* mutants, and we therefore would not hypothesize axonal debris to contribute to the
271 misguidance of RGC axons in *lh3* mutants.

272 Second, our live cell imaging reveals that a small group of axon fascicles exhibit strongly
273 directed growth toward the midline by 16 hpt and subsequently extends across rapidly (Fig. 3D-
274 E, Supplementary Movie 1, white arrowheads). Additional fascicles of axons continue to grow and
275 follow the growth of the axons that initially crossed the midline (Fig. 3F, Supplementary Movie 1).
276 These axons grow along a path that almost completely overlaps with their original path (Fig. 4D),
277 and strongly suggests that there are factors expressed from cells associated with that projection
278 that direct regrowing RGC axons during optic nerve regeneration.

279 **A novel role for oligodendrocytes in axon guidance during axon regeneration**

280 To determine the relevant cell type through which *lh3* is functioning during optic nerve
281 regeneration, we use cell-type specific transgenic rescue. Based on the *lh3* and *col18a1* mRNA
282 expression in the optic chiasm (Fig. 2G-I, 6A), we hypothesized that the relevant cell type would
283 be one found in that region during the initial stages of regeneration. We observe macrophages
284 and microglia dynamically infiltrating the chiasm and surrounding regenerating axonal growth (Fig.
285 5A). *Tg(mpeg:lh3-myc)* expression fails to rescue aberrant axonal growth in *lh3* mutants,
286 suggesting that *lh3* expression needs to be more specifically spatially regulated (Fig. 5D). We
287 therefore examined oligodendrocytes and observe oligodendrocyte lineage cells present in the
288 optic chiasm and we detect *mbpa* mRNA indicative of myelinating oligodendrocytes along the
289 degenerating axons (Fig. 5B-C). We find that *lh3* expression from a *Tg(sox10:lh3-mkate)*
290 transgene restores RGC regrowth across the midline in *lh3* mutants (Fig 5E). However, the
291 transgenic tools we employed here do not allow is to distinguish whether oligodendrocyte
292 precursor cells or mature oligodendrocytes were the relevant cell type for *lh3* and *col18a1,* as
293 *sox10* and *olig2* are both transcription factors that are expressed in all oligodendrocyte lineage
294 cells (Bergles and Richardson, 2015; Ackerman and Monk, 2016). Previous studies implicate
295 oligodendrocytes to play roles in remyelination (Wang *et al.*, 2020; Mendonça *et al.*, 2021) and
296 axon repulsion or inhibition via myelin-associated glycoprotein (McKerracher *et al.*, 1994;
297 Mukhopadhyay *et al.*, 1994), NogoA (Chen *et al.*, 2000; GrandPré *et al.*, 2000), oligodendrocyte-
298 myelin glycoprotein (K. C. Wang *et al.*, 2002) and semaphorin 4D (Moreau-Fauvarque *et al.*,
299 2003). From our results, we propose a mechanism in which Lh3 and Col18a1 expressed in
300 oligodendrocytes mediate axon attraction to direct regenerating RGC axons along their original
301 path, suggesting a novel role for oligodendrocytes in CNS regeneration.

302 **A molecular mechanism for *lh3* and *col18a1* in specifying a regenerative path**

303 We identify *lh3* to be required to direct regenerating RGC axons toward and across the
304 optic chiasm (Fig 1). We then determined that *col18a1* is also critical for directing RGC axons

305 during optic nerve regeneration, but not another basement membrane *col4a5* or fibrillar *col7a1*,
306 which demonstrates a specific role for *col18a1* in optic nerve regeneration (Fig 6, Fig S2). But the
307 question remains: what are the mechanisms by which Lh3 and Col18a1 target RGC axons to their
308 original path? We cannot exclude a possible mechanism involving RGC axons directly interacting
309 with Col18a1 in the extracellular matrix through integrins (Elango *et al.*, 2022). Transcriptomic
310 analysis of RGCs at different stages of regeneration in adult zebrafish shows that several integrins
311 are upregulated as axons grow toward and across the midline (Dhara *et al.*, 2019). Therefore, the
312 spatial and temporal specificity of Lh3 and Col18a1 expression could establish the regenerative
313 path for regrowing RGC axons independent of any other guidance cues.

314 But in addition to playing structural roles, there is growing evidence showing a critical role
315 for extracellular matrix proteins to bind and regulate the spatial distribution of axon guidance
316 molecules in the extracellular space. For decades, glycosaminoglycans, such as heparan sulfate
317 proteoglycans, have been known to regulate the extracellular localization of Slit repulsive
318 guidance cues to affect axon guidance in development (Wang and Denburg, 1992; Johnson *et*
319 *al.*, 2004; Smart *et al.*, 2011). More specifically, *col4a5* has been shown to be critical during
320 development of the retinotectal projection for localizing Slit1 expression in the superficial layers
321 of the optic tectum, which mediates lamina-specific axon targeting (Xiao and Baier, 2007; Xiao *et*
322 *al.*, 2011). During motor nerve regeneration, spatially restricted *col4a5* and *lh3* are required in a
323 subset of Schwann cells to possibly create a Slit1a gradient that directs dorsal nerve axons to
324 their original projection paths (Isaacman-Beck *et al.*, 2015; Murphy, Isaacman-Beck and Granato,
325 2022). In this study, our results describe a similar mechanism where *lh3* is required to direct
326 regrowing RGC axons toward the midline along their original path, but here, we find in optic nerve
327 regeneration that Lh3 potentially acts through Col18a1, not Col4a5. What are possible guidance
328 cues that Col18a1 could be spatially regulating? Col18a1 has three isoforms and within the long
329 isoform is a Frizzled-like domain that has been shown to interact with Wnt molecules (Quélard *et*

330 *al.*, 2008). Moreover, Wnt signaling has been implicated in both promoting as well as repelling
331 axonal growth in spinal cord and optic nerve regeneration (Yin *et al.*, 2008; Hollis and Zou, 2012;
332 Yam and Charron, 2013; Strand *et al.*, 2016; Patel, Park and Hackam, 2017; Wehner *et al.*, 2017).
333 Therefore, we propose another potential mechanism in which Lh3 is required for Col18a1
334 expression that possibly spatially restricts Wnts in the extracellular space along the original RGC
335 axonal projection to direct regenerating RGC axons during optic nerve regeneration. Altogether,
336 our studies demonstrate that live cell imaging of optic nerve regeneration in larval zebrafish allows
337 for unprecedented visualization of axonal growth dynamics and potential interactions with other
338 cell types in the optic chiasm. Our data here reveal a glial derived molecular pathway that directs
339 regenerating RGC axons across the optic chiasm during optic nerve regeneration, furthering our
340 understanding of the cellular and molecular mechanisms that promote robust functional optic
341 nerve regeneration.

342 **Methods**

343 **Fish lines and maintenance**

344 All zebrafish (*Danio rerio*) work was performed in compliance with the University of Pennsylvania
345 Institutional Animal Care and Use Committee regulations and raised as previously described
346 (Mullins *et al.*, 1994). All transgenic lines were maintained in the Tupfel long fin genetic
347 background except the *col18a1* line, which were maintain in the AB background. The following
348 transgenic lines and mutants were used: *lh3*^{TV2O5} (Schneider and Granato, 2006), *col18a1*
349 (Isaacman-Beck *et al.*, 2015), *col4a5*^{s510} (Xiao and Baier, 2007), *col7a1*^{sa3473}, *Tg(hsp:lh30-myc)*
350 (Isaacman-Beck *et al.*, 2015), *Tg(sox10:lh3-mkate)* (Isaacman-Beck *et al.*, 2015), *Tg(isl2b:GFP)*
351 (Pittman, Law and Chien, 2008), *Tg(olig2:dsred)* (Kucenas *et al.*, 2008),
352 *Tg*(*mpeg1:Gal4FF*)^{gl25} (Ellett *et al.*, 2011) and *Tg*(*UAS:nfsB-mCherry*)^{c264} (Davison *et al.*, 2007).
353

354 Adult zebrafish and embryos were raised at 28°C on a 14-h:10-h light:dark cycle, or 29°C for
355 larvae in PTU E3, see Transection Assay.
356

357 To generate *Tg(mpeg1.1:lh3-myc)*, Gateway cloning was employed to combine *lh3-myc* into a
358 pDest vector with the mpeg1.1 promoter and Tol2 transposon sites. Tol2 transgenesis was
359 performed as previously described(Suster *et al.*, 2009) into 1-cell stage embryos from *lh3*
360 heterozygous incrosses. Transgenic lines were identified by genotyping for the transgene with
361 forward primer ACAGTCTCTTGCGTCATCAAAACC and reverse primer
362 TGATCACCAGCAGCTCATTG.
363

364 **Transection Assay**

365 Optic nerve transection assays were performed as previously described(Harvey, Baxter and
366 Granato, 2019, 2023). Briefly, to inhibit melanocyte pigmentation, larvae were raised in

367 phenylthiourea (PTU, 0.2mM in E3 medium) in the dark at 29°C beginning at 1 dpf. For live cell
368 imaging and distal transections, larvae were anesthetized in PTU E3 plus 0.0053% tricaine then
369 mounted in 2.5% low-melt agarose (SeaPlaque, Lonza) prepared with PTU E3 plus 0.016%
370 tricaine ventral-up on a glass microscopy slide. Then one eye was completely removed using
371 forceps at 4 dpf. Larvae recovered in Ringer's solution and then were kept in PTU E3 at 29°C
372 until transected. At 5 dpf, larvae were anesthetized, mounted in agarose, and then optic nerve
373 transections were performed on an Olympus SZX16 fluorescent microscope or a dissecting
374 microscope with a NightSea Stereo Microscope Fluorescence Adapter (RB-GO only wavelength
375 set, bandpass filter) using a sharpened tungsten needle (Fine Science Tools, Tip Diameter:
376 0.001mm, Rod Diameter: 0.125mm). Optic nerves were transected at the region of the nerve
377 distal to it exiting the eye, yet proximal to the optic chiasm. Following injuries, larvae were removed
378 from the agarose, allowed to recover in Ringer's solution with 0.2mM PTU, then returned to 0.2mM
379 PTU, E3 medium at 29°C. Larvae were inspected for transection efficiency at 16-18 hpt, except
380 larvae that were fixed at early post transection timepoints, and only larvae with complete optic
381 nerve transections with no visible intact axons remaining from the eye to the tectum were kept
382 until fixation at later designated timepoints.

383 **Heat Shock-Induced *lh3* Rescue**

384 To induce expression of Lh3 from *Tg(hsp:lh3-myc)* transgene, during development: Embryos were
385 developmentally staged in the late afternoon. No more than 6 embryos were placed per tube in
386 PCR strip-tubes. Tubes were incubated in a thermal cycler at 28°C until embryos would reach
387 11.66 hpf, then heated to 38°C for 10 minutes, then held at 28°C until they could be removed from
388 the tubes.

389 To induce expression of Lh3 from Tg(hsp:lh3-myc) transgene, during regeneration: Larvae at 5
390 dpf homozygous for the Tg(hsp:lh3-myc) transgene were placed only one per tube in PCR strip-

391 tubes. Tubes were incubated in a thermal cycler at 38°C for 30min then held at 29°C until they
392 could be removed from the tubes. Larvae were transected 4-5 hours later.

393 **Immunostaining**

394 Larvae were stained using methods modified from those previously described (Randlett *et al.*,
395 2015). Briefly, larvae were fixed in 4% PFA in PBS overnight at 4°C. Larvae were washed in PBS
396 + 0.25% Triton (PBT), incubated in 150mM Tris-HCl pH 9.0 for 15 min at 70°C, then washed in
397 PBT. Larvae were permeabilized in 0.05% Trypsin-EDTA for 5 min on ice , washed in PBT, blocked
398 in PBT containing 1% bovine serum albumin (BSA), 2% normal goat serum (NGS) and 1%
399 dimethyl sulfoxide (DMSO), and then incubated in primary and secondary antibodies overnight at
400 4°C in PBT containing 1% BSA and 1% DMSO. Stained larvae were stored and mounted in
401 Vectashield (Vector Laboratories) for imaging using confocal microscopy. For static timepoint
402 analysis of *lh3* and *col18a1* mutants, primary antibodies used were mouse anti-GFP (JL-8, 1:200,
403 Takara Bio), and secondary antibodies used were goat anti-mouse Alexa 488 (1:500, Molecular
404 Probes). For static timepoint analysis of macrophages/microglia, primary antibodies used were
405 mouse anti-GFP (JL-8, 1:200, Takara Bio), rabbit anti-RFP (1:200, Abcam ab62341) and
406 secondary antibodies used were goat anti-mouse Alexa 488 (1:500, Molecular Probes) and goat
407 anti-rabbit Alexa 594 (1:500, Molecular Probes). For static timepoint analysis of oligodendrocytes,
408 primary antibodies used were rabbit anti-GFP (1:500, Molecular Probes), mouse anti-dsred
409 (1:500, BD Pharmingen) and secondary antibodies used were goat anti-rabbit 488 (1:500,
410 Molecular Probes) and goat anti-mouse Alexa 594 (1:500, Molecular Probes).

411 **Fluorescent *in situ* Hybridization with Hybridization Chain Reaction (HCR)**

412 *Lh3 (plod3), col18a1 and mbpa* mRNA expression were detected using fluorescent *in situ*
413 hybridization with HCR (Molecular Instruments, Los Angeles, CA, USA)(Choi *et al.*, 2018). HCR
414 probes, buffers, and hairpins were purchased from Molecular Instruments. *Tg(isl2b:GFP)* larvae
415 were fixed at 5 dpf with 4% paraformaldehyde in PBS overnight at 4°C. No antibody staining was

416 required together with in situ HCR. The staining was performed as previously described(Shainer
417 *et al.*, 2023).

418 **Static Confocal Imaging, Processing and Analysis**

419 Larvae were imaged on a Zeiss 880 confocal microscope using a 20× objective. Airyscan super-
420 resolution settings were used to obtain Figures 5G and 6B. Image stacks of optic chiasms or tecta
421 were compressed into maximum intensity projections. All images were adjusted for brightness
422 and contrast in Adobe Photoshop CS5, and color assigned using Fiji.

423 **Live Cell Imaging, Processing and Analysis**

424 Larvae were anesthetized in PTU E3 with 0.0053% tricaine then mounted in 2.5% low-melt
425 agarose (SeaPlaque, Lonza) prepared with PTU E3 plus 0.016% tricaine ventral-up on a glass
426 microscopy slide. Then, a portion of the jaw, including the Meckel's cartilage, palatoquadrate, and
427 the most distal parts of the basihyal and ceratohyal structures, as well as one eye were carefully
428 removed using forceps at 4 dpf. Care was taken so as not to damage the heart. Larvae recovered
429 in Ringer's solution and then were kept in PTU E3 at 29°C until transected. At 5 dpf, larvae were
430 anesthetized again, mounted in agarose, and then optic nerve transections were performed.
431 Larvae recovered in Ringer's solution and then were kept in PTU E3 at 29°C until imaged for live
432 cell imaging. For live imaging, larvae were mounted ventral side up in 35mm glass-bottomed Petri
433 dishes in 1.5% low-melt agarose with 0.016% tricaine. Larvae were imaged using a Leica SP8
434 confocal microscope with the resonant scanner on, equipped with a petri dish heater and heated
435 water perfusion so fresh E3 water flowed through the petri dish and the temperature was kept
436 constant at around 28°C during the imaging session. Larvae were imaged from the ventral side
437 of the brain, which was not covered by any jaw tissue. Image stacks were acquired every 10-15
438 minutes with a 20x 1.0 NA lens. All images were adjusted for brightness and contrast, and color
439 assigned using Fiji.

440 To determine the time of growth initiation extending from the proximal stump of transected RGC
441 axons, we recorded in which frame axonal extension longer than 1um occurred that continued to
442 extend for another subsequent frame.
443 To measure the angle of the original path before transection to the end of distinct axon fascicles,
444 we first rotated the images so that parasphenoid cartilage was precisely aligned vertically against
445 a straight line drawn in Fiji. A circle with a radius of 80 uM centered where RGC axons exit the
446 eye was drawn within Fiji using a Make Oval Macro in timelapse image sequences. Axons and
447 fascicles terminating farther than the 80 uM region of interest at 20 hpt were used for measuring.
448 First the angle of the original path to the parasphenoid was determined using frames before
449 Wallerian degeneration was complete. Then the angle of the axons and fascicles to the
450 parasphenoid were determined, and then the difference was calculated and graphed.

451 **Statistical Analysis**

452 Data were imported into GraphPad Prism for analysis. Statistical analysis was performed as
453 indicated throughout the text.
454

455 ## Acknowledgments

456 We would like to thank Dr. Andrea Stout of the UPenn Cell and Developmental Biology Microscopy
457 Core, as well as Dr. Gordon Ruthel of the Penn Vet Imaging Core for providing technical
458 assistance. We thank all members of the Granato laboratory for comments and discussion.
459

460 ## Funding

461 This work was supported by grants from the National Institutes of Health to B.M.H. (EY032593)
462 and M.G. (EY024861 and NS097914).
463

464 ## Author Contributions

B.M.H. and M.G. conceptualized the experiments; B.M.H. M.B, and A.M.G. performed and analyzed experiments; B.M.H. wrote the original draft. All authors contributed to editing and revision of the paper.

Data Availability

All relevant data are within the article and its supplementary information files.

Competing interests

The authors declare no competing interests.

References

Ackerman, S.D. and Monk, K.R. (2016) “The scales and tales of myelination: using zebrafish and mouse to study myelinating glia,” *Brain Research*, 1641(Pt A), pp. 79–91. Available at: https://doi.org/10.1016/j.brainres.2015.10.011.

Bergles, D.E. and Richardson, W.D. (2015) “Oligodendrocyte Development and Plasticity,” *Cold Spring Harbor Perspectives in Biology*, 8(2), p. a020453. Available at: https://doi.org/10.1101/cshperspect.a020453.

Berkelaar, M. *et al.* (1994) “Axotomy results in delayed death and apoptosis of retinal ganglion cells in adult rats,” *The Journal of Neuroscience: The Official Journal of the Society for Neuroscience*, 14(7), pp. 4368–4374.

Berry, M., Ahmed, Z. and Logan, A. (2019) “Return of function after CNS axon regeneration: Lessons from injury-responsive intrinsically photosensitive and alpha retinal ganglion cells,” *Progress in Retinal and Eye Research*, 71, pp. 57–67. Available at: https://doi.org/10.1016/j.preteyeres.2018.11.006.

Bhatt, D.H. *et al.* (2004) “Cyclic AMP-induced repair of zebrafish spinal circuits,” *Science (New York, N.Y.)*, 305(5681), pp. 254–258. Available at: https://doi.org/10.1126/science.1098439.

Bremer, J. *et al.* (2019) “The ubiquitin ligase PHR promotes directional regrowth of spinal zebrafish axons,” *Communications Biology*, 2, p. 195. Available at: https://doi.org/10.1038/s42003-019-0434-2.

Brennan, F.H. *et al.* (2022) “Microglia coordinate cellular interactions during spinal cord repair in mice,” *Nature Communications*, 13(1), p. 4096. Available at: https://doi.org/10.1038/s41467-022-31797-0.

Brockerhoff, S.E. *et al.* (1995) “A behavioral screen for isolating zebrafish mutants with visual system defects,” *Proceedings of the National Academy of Sciences of the United States of America*, 92(23), pp. 10545–10549.

Brösamle, C. and Halpern, M.E. (2002) “Characterization of myelination in the developing zebrafish,” *Glia*, 39(1), pp. 47–57. Available at: https://doi.org/10.1002/glia.10088.

Ceci, M.L. *et al.* (2014) “Axon-Schwann cell interactions during peripheral nerve regeneration in zebrafish larvae,” *Neural Development*, 9, p. 22. Available at: https://doi.org/10.1186/1749-8104-9-22.

Chen, M.S. *et al.* (2000) “Nogo-A is a myelin-associated neurite outgrowth inhibitor and an antigen for monoclonal antibody IN-1,” *Nature*, 403(6768), pp. 434–439. Available at: https://doi.org/10.1038/35000219.

Choi, H.M.T. *et al.* (2018) “Third-generation in situ hybridization chain reaction: multiplexed, quantitative, sensitive, versatile, robust,” *Development (Cambridge, England)*, 145(12), p. dev165753. Available at: https://doi.org/10.1242/dev.165753.

511 Davison, J.M. *et al.* (2007) “Transactivation from Gal4-VP16 transgenic insertions for tissue-
512 specific cell labeling and ablation in zebrafish,” *Developmental Biology*, 304(2), pp. 811–824.
513 Available at: https://doi.org/10.1016/j.ydbio.2007.01.033.

514 Dhara, S.P. *et al.* (2019) “Cellular reprogramming for successful CNS axon regeneration is
515 driven by a temporally changing cast of transcription factors,” *Scientific Reports*, 9(1), p. 14198.
516 Available at: https://doi.org/10.1038/s41598-019-50485-6.

517 Easter, S.S. and Nicola, G.N. (1996) “The development of vision in the zebrafish (Danio rerio),”
518 *Developmental Biology*, 180(2), pp. 646–663.

519 Elango, J. *et al.* (2022) “The Molecular Interaction of Collagen with Cell Receptors for Biological
520 Function,” *Polymers*, 14(5), p. 876. Available at: https://doi.org/10.3390/polym14050876.

521 Ellett, F. *et al.* (2011) “mpeg1 promoter transgenes direct macrophage-lineage expression in
522 zebrafish,” *Blood*, 117(4), pp. e49-56. Available at: https://doi.org/10.1182/blood-2010-10-
523 314120.

524 Fitch, M.T. and Silver, J. (2008) “CNS injury, glial scars, and inflammation: Inhibitory extracellular
525 matrices and regeneration failure,” *Experimental Neurology*, 209(2), pp. 294–301. Available at:
526 https://doi.org/10.1016/j.expneurol.2007.05.014.

527 Fukai, N. *et al.* (2002) “Lack of collagen XVIII/endostatin results in eye abnormalities,” *The*
528 *EMBO journal*, 21(7), pp. 1535–1544. Available at: https://doi.org/10.1093/emboj/21.7.1535.

529 Gahtan, E., Tanger, P. and Baier, H. (2005) “Visual prey capture in larval zebrafish is controlled
530 by identified reticulospinal neurons downstream of the tectum,” *The Journal of Neuroscience:*
531 *The Official Journal of the Society for Neuroscience*, 25(40), pp. 9294–9303. Available at:
532 https://doi.org/10.1523/JNEUROSCI.2678-05.2005.

533 Goldberg, J.L. *et al.* (2002) “Retinal ganglion cells do not extend axons by default: promotion by
534 neurotrophic signaling and electrical activity,” *Neuron*, 33(5), pp. 689–702. Available at:
535 https://doi.org/10.1016/s0896-6273(02)00602-5.

536 GrandPré, T. *et al.* (2000) “Identification of the Nogo inhibitor of axon regeneration as a
537 Reticulon protein,” *Nature*, 403(6768), pp. 439–444. Available at:
538 https://doi.org/10.1038/35000226.

539 Harvey, B.M., Baxter, M. and Granato, M. (2019) “Optic nerve regeneration in larval zebrafish
540 exhibits spontaneous capacity for retinotopic but not tectum specific axon targeting,” *PloS One*,
541 14(6), p. e0218667. Available at: https://doi.org/10.1371/journal.pone.0218667.

542 Harvey, B.M., Baxter, M. and Granato, M. (2023) “Assaying Optic Nerve Regeneration in Larval
543 Zebrafish,” *Methods in Molecular Biology (Clifton, N.J.)*, 2636, pp. 191–203. Available at:
544 https://doi.org/10.1007/978-1-0716-3012-9_10.

545 Heikkinen, J. *et al.* (2000) “Lysyl hydroxylase 3 is a multifunctional protein possessing collagen
546 glucosyltransferase activity,” *The Journal of Biological Chemistry*, 275(46), pp. 36158–36163.
547 Available at: https://doi.org/10.1074/jbc.M006203200.

548 Hollis, E.R. and Zou, Y. (2012) “Expression of the Wnt signaling system in central nervous
549 system axon guidance and regeneration,” *Frontiers in Molecular Neuroscience*, 5, p. 5. Available
550 at: https://doi.org/10.3389/fnmol.2012.00005.

551 Horder, T.J. (1971) “The course of recovery of the retinotectal projection during regeneration of
552 the fish optic nerve,” *The Journal of Physiology*, 217 Suppl, pp. 53P-54P.

553 Isaacman-Beck, J. *et al.* (2015) “The Ih3 Glycosyltransferase Directs Target-Selective Peripheral
554 Nerve Regeneration,” *Neuron*, 88(4), pp. 691–703. Available at:
555 https://doi.org/10.1016/j.neuron.2015.10.004.

556 Johnson, K.G. *et al.* (2004) “Axonal heparan sulfate proteoglycans regulate the distribution and
557 efficiency of the repellent slit during midline axon guidance,” *Current biology: CB*, 14(6), pp.
558 499–504. Available at: https://doi.org/10.1016/j.cub.2004.02.005.

559 Kucenas, S. *et al.* (2008) “CNS-derived glia ensheath peripheral nerves and mediate motor root
560 development,” *Nature Neuroscience*, 11(2), pp. 143–151. Available at:
561 https://doi.org/10.1038/nn2025.

562 Kurimoto, T. *et al.* (2010) “Long-distance axon regeneration in the mature optic nerve:
563 contributions of oncomodulin, cAMP, and pten gene deletion,” *The Journal of Neuroscience: The*
564 *Official Journal of the Society for Neuroscience*, 30(46), pp. 15654–15663. Available at:
565 https://doi.org/10.1523/JNEUROSCI.4340-10.2010.

566 Leon, S. *et al.* (2000) “Lens injury stimulates axon regeneration in the mature rat optic nerve,”
567 *The Journal of Neuroscience: The Official Journal of the Society for Neuroscience*, 20(12), pp.
568 4615–4626.

569 Lewis, G.M. and Kucenas, S. (2014) “Perineurial glia are essential for motor axon regrowth
570 following nerve injury,” *The Journal of Neuroscience: The Official Journal of the Society for*
571 *Neuroscience*, 34(38), pp. 12762–12777. Available at:
572 https://doi.org/10.1523/JNEUROSCI.1906-14.2014.

573 Luo, X. *et al.* (2013) “Three-dimensional evaluation of retinal ganglion cell axon regeneration
574 and pathfinding in whole mouse tissue after injury,” *Experimental Neurology*, 247, pp. 653–662.
575 Available at: https://doi.org/10.1016/j.expneurol.2013.03.001.

576 Marquart, G.D. *et al.* (2017) “High-precision registration between zebrafish brain atlases using
577 symmetric diffeomorphic normalization,” *GigaScience*, 6(8), pp. 1–15. Available at:
578 https://doi.org/10.1093/gigascience/gix056.

579 Martin, S.M. *et al.* (2010) “Wallerian degeneration of zebrafish trigeminal axons in the skin is
580 required for regeneration and developmental pruning,” *Development (Cambridge, England)*,
581 137(23), pp. 3985–3994. Available at: https://doi.org/10.1242/dev.053611.

582 McKerracher, L. *et al.* (1994) “Identification of myelin-associated glycoprotein as a major myelin-
583 derived inhibitor of neurite growth,” *Neuron*, 13(4), pp. 805–811. Available at:
584 https://doi.org/10.1016/0896-6273(94)90247-x.

585 Mendonça, H.R. *et al.* (2021) “Myelination of regenerating optic nerve axons occurs in
586 conjunction with an increase of the oligodendrocyte precursor cell population in the adult mice,”

587 *Brain Research Bulletin*, 166, pp. 150–160. Available at:
588 https://doi.org/10.1016/j.brainresbull.2020.11.012.

589 Moore, D.L. *et al.* (2009) “KLF family members regulate intrinsic axon regeneration ability,”
590 *Science (New York, N.Y.)*, 326(5950), pp. 298–301. Available at:
591 https://doi.org/10.1126/science.1175737.

592 Moreau-Fauvarque, C. *et al.* (2003) “The transmembrane semaphorin Sema4D/CD100, an
593 inhibitor of axonal growth, is expressed on oligodendrocytes and upregulated after CNS lesion,”
594 *The Journal of Neuroscience: The Official Journal of the Society for Neuroscience*, 23(27), pp.
595 9229–9239. Available at: https://doi.org/10.1523/JNEUROSCI.23-27-09229.2003.

596 Mukhopadhyay, G. *et al.* (1994) “A novel role for myelin-associated glycoprotein as an inhibitor
597 of axonal regeneration,” *Neuron*, 13(3), pp. 757–767. Available at: https://doi.org/10.1016/0896-
598 6273(94)90042-6.

599 Mullins, M.C. *et al.* (1994) “Large-scale mutagenesis in the zebrafish: in search of genes
600 controlling development in a vertebrate,” *Current biology: CB*, 4(3), pp. 189–202.

601 Murphy, P.L., Isaacman-Beck, J. and Granato, M. (2022) “Robo2 Drives Target-Selective
602 Peripheral Nerve Regeneration in Response to Glia-Derived Signals,” *The Journal of*
603 *Neuroscience: The Official Journal of the Society for Neuroscience*, 42(5), pp. 762–776.
604 Available at: https://doi.org/10.1523/JNEUROSCI.1528-21.2021.

605 Murray, M. (1976) “Regeneration of retinal axons into the goldfish optic tectum,” *The Journal of*
606 *Comparative Neurology*, 168(2), pp. 175–195. Available at:
607 https://doi.org/10.1002/cne.901680202.

608 Nogueira-Rodrigues, J. *et al.* (2022) “Rewired glycosylation activity promotes scarless
609 regeneration and functional recovery in spiny mice after complete spinal cord transection,”
610 *Developmental Cell*, 57(4), pp. 440-450.e7. Available at:
611 https://doi.org/10.1016/j.devcel.2021.12.008.

612 Norsworthy, M.W. *et al.* (2017) “Sox11 Expression Promotes Regeneration of Some Retinal
613 Ganglion Cell Types but Kills Others,” *Neuron*, 94(6), pp. 1112-1120.e4. Available at:
614 https://doi.org/10.1016/j.neuron.2017.05.035.

615 Park, K.K. *et al.* (2008) “Promoting axon regeneration in the adult CNS by modulation of the
616 PTEN/mTOR pathway,” *Science (New York, N.Y.)*, 322(5903), pp. 963–966. Available at:
617 https://doi.org/10.1126/science.1161566.

618 Park, K.K. *et al.* (2017) “Retinal ganglion cell survival and axon regeneration after optic nerve
619 injury in naked mole-rats,” *The Journal of Comparative Neurology*, 525(2), pp. 380–388.
620 Available at: https://doi.org/10.1002/cne.24070.

621 Patel, A.K., Park, K.K. and Hackam, A.S. (2017) “Wnt signaling promotes axonal regeneration
622 following optic nerve injury in the mouse,” *Neuroscience*, 343, pp. 372–383. Available at:
623 https://doi.org/10.1016/j.neuroscience.2016.12.020.

Pernet, Vincent *et al.* (2013) “Long-distance axonal regeneration induced by CNTF gene transfer is impaired by axonal misguidance in the injured adult optic nerve,” *Neurobiology of Disease*, 51, pp. 202–213. Available at: https://doi.org/10.1016/j.nbd.2012.11.011.

Pernet, V. *et al.* (2013) “Misguidance and modulation of axonal regeneration by Stat3 and Rho/ROCK signaling in the transparent optic nerve,” *Cell Death & Disease*, 4, p. e734. Available at: https://doi.org/10.1038/cddis.2013.266.

Pittman, A.J., Law, M.-Y. and Chien, C.-B. (2008) “Pathfinding in a large vertebrate axon tract: isotypic interactions guide retinotectal axons at multiple choice points,” *Development (Cambridge, England)*, 135(17), pp. 2865–2871. Available at: https://doi.org/10.1242/dev.025049.

Quélard, D. *et al.* (2008) “A cryptic frizzled module in cell surface collagen 18 inhibits Wnt/beta-catenin signaling,” *PloS One*, 3(4), p. e1878. Available at: https://doi.org/10.1371/journal.pone.0001878.

Randlett, O. *et al.* (2015) “Whole-brain activity mapping onto a zebrafish brain atlas,” *Nature Methods*, 12(11), pp. 1039–1046. Available at: https://doi.org/10.1038/nmeth.3581.

Risteli, M. *et al.* (2004) “Characterization of collagenous peptides bound to lysyl hydroxylase isoforms,” *The Journal of Biological Chemistry*, 279(36), pp. 37535–37543. Available at: https://doi.org/10.1074/jbc.M405638200.

Rosenberg, A.F. *et al.* (2012) “In vivo nerve-macrophage interactions following peripheral nerve injury,” *The Journal of Neuroscience: The Official Journal of the Society for Neuroscience*, 32(11), pp. 3898–3909. Available at: https://doi.org/10.1523/JNEUROSCI.5225-11.2012.

Salo, A.M. and Myllyharju, J. (2021) “Prolyl and lysyl hydroxylases in collagen synthesis,” *Experimental Dermatology*, 30(1), pp. 38–49. Available at: https://doi.org/10.1111/exd.14197.

Schneider, V.A. and Granato, M. (2006) “The myotomal diwanka (lh3) glycosyltransferase and type XVIII collagen are critical for motor growth cone migration,” *Neuron*, 50(5), pp. 683–695. Available at: https://doi.org/10.1016/j.neuron.2006.04.024.

Shainer, I. *et al.* (2023) “A single-cell resolution gene expression atlas of the larval zebrafish brain,” *Science Advances*, 9(8), p. eade9909. Available at: https://doi.org/10.1126/sciadv.ade9909.

Smart, A.D. *et al.* (2011) “Heparan sulfate proteoglycan specificity during axon pathway formation in the Drosophila embryo,” *Developmental Neurobiology*, 71(7), pp. 608–618. Available at: https://doi.org/10.1002/dneu.20854.

Smith, P.D. *et al.* (2009) “SOCS3 deletion promotes optic nerve regeneration in vivo,” *Neuron*, 64(5), pp. 617–623. Available at: https://doi.org/10.1016/j.neuron.2009.11.021.

Strand, N.S. *et al.* (2016) “Wnt/β-catenin signaling promotes regeneration after adult zebrafish spinal cord injury,” *Biochemical and Biophysical Research Communications*, 477(4), pp. 952–956. Available at: https://doi.org/10.1016/j.bbrc.2016.07.006.

661 Suster, M.L. *et al.* (2009) “Transgenesis in zebrafish with the tol2 transposon system,” *Methods*
662 *in Molecular Biology (Clifton, N.J.)*, 561, pp. 41–63. Available at: https://doi.org/10.1007/978-1-
663 60327-019-9_3.

664 Suzuki, O.T. *et al.* (2002) “Molecular analysis of collagen XVIII reveals novel mutations,
665 presence of a third isoform, and possible genetic heterogeneity in Knobloch syndrome,”
666 *American Journal of Human Genetics*, 71(6), pp. 1320–1329. Available at:
667 https://doi.org/10.1086/344695.

668 Taler, K. *et al.* (2019) “Lysyl hydroxylase 3 is required for normal lens capsule formation and
669 maintenance of lens epithelium integrity and fate,” *Developmental Biology* [Preprint]. Available
670 at: https://doi.org/10.1016/j.ydbio.2019.10.020.

671 Vargas, M.E. and Barres, B.A. (2007) “Why is Wallerian degeneration in the CNS so slow?,”
672 *Annual Review of Neuroscience*, 30, pp. 153–179. Available at:
673 https://doi.org/10.1146/annurev.neuro.30.051606.094354.

674 Villegas-Pérez, M.P. *et al.* (1993) “Rapid and protracted phases of retinal ganglion cell loss
675 follow axotomy in the optic nerve of adult rats,” *Journal of Neurobiology*, 24(1), pp. 23–36.
676 Available at: https://doi.org/10.1002/neu.480240103.

677 Waller, A. (1851) “Experiments on the Section of the Glosso-Pharyngeal and Hypoglossal
678 Nerves of the Frog, and Observations of the Alterations Produced Thereby in the Structure of
679 Their Primitive Fibres,” *Edinburgh Medical and Surgical Journal*, 76(189), pp. 369–376.

680 Wang, C. *et al.* (2002) “The third activity for lysyl hydroxylase 3: galactosylation of hydroxylysyl
681 residues in collagens in vitro,” *Matrix Biology: Journal of the International Society for Matrix*
682 *Biology*, 21(7), pp. 559–566.

683 Wang, J. *et al.* (2020) “Robust Myelination of Regenerated Axons Induced by Combined
684 Manipulations of GPR17 and Microglia,” *Neuron*, 108(5), pp. 876-886.e4. Available at:
685 https://doi.org/10.1016/j.neuron.2020.09.016.

686 Wang, K.C. *et al.* (2002) “Oligodendrocyte-myelin glycoprotein is a Nogo receptor ligand that
687 inhibits neurite outgrowth,” *Nature*, 417(6892), pp. 941–944. Available at:
688 https://doi.org/10.1038/nature00867.

689 Wang, L. and Denburg, J.L. (1992) “A role for proteoglycans in the guidance of a subset of
690 pioneer axons in cultured embryos of the cockroach,” *Neuron*, 8(4), pp. 701–714. Available at:
691 https://doi.org/10.1016/0896-6273(92)90091-q.

692 Wehner, D. *et al.* (2017) “Wnt signaling controls pro-regenerative Collagen XII in functional
693 spinal cord regeneration in zebrafish,” *Nature Communications*, 8(1), p. 126. Available at:
694 https://doi.org/10.1038/s41467-017-00143-0.

695 Wullink, B. *et al.* (2018) “Type VII Collagen in the Human Accommodation System: Expression
696 in Ciliary Body, Zonules, and Lens Capsule,” *Investigative Ophthalmology & Visual Science*,
697 59(2), pp. 1075–1083. Available at: https://doi.org/10.1167/iovs.17-23425.

698 Xiao, T. *et al.* (2011) “Assembly of lamina-specific neuronal connections by slit bound to type IV
699 collagen,” *Cell*, 146(1), pp. 164–176. Available at: https://doi.org/10.1016/j.cell.2011.06.016.

Xiao, T. and Baier, H. (2007) “Lamina-specific axonal projections in the zebrafish tectum require the type IV collagen Dragnet,” *Nature Neuroscience*, 10(12), pp. 1529–1537. Available at: https://doi.org/10.1038/nn2002.

Yam, P.T. and Charron, F. (2013) “Signaling mechanisms of non-conventional axon guidance cues: the Shh, BMP and Wnt morphogens,” *Current Opinion in Neurobiology*, 23(6), pp. 965–973. Available at: https://doi.org/10.1016/j.conb.2013.09.002.

Yin, Y. *et al.* (2009) “Oncomodulin links inflammation to optic nerve regeneration,” *Proceedings of the National Academy of Sciences of the United States of America*, 106(46), pp. 19587–19592. Available at: https://doi.org/10.1073/pnas.0907085106.

Yin, Y. and Benowitz, L.I. (2018) “In Vitro and In Vivo Methods for Studying Retinal Ganglion Cell Survival and Optic Nerve Regeneration,” *Methods in Molecular Biology (Clifton, N.J.)*, 1695, pp. 187–205. Available at: https://doi.org/10.1007/978-1-4939-7407-8_16.

Yin, Z.-S. *et al.* (2008) “Repair effect of Wnt3a protein on the contused adult rat spinal cord,” *Neurological Research*, 30(5), pp. 480–486. Available at: https://doi.org/10.1179/174313208X284133.

Yiu, G. and He, Z. (2006) “Glial inhibition of CNS axon regeneration,” *Nature Reviews. Neuroscience*, 7(8), pp. 617–627. Available at: https://doi.org/10.1038/nrn1956.

Zeller, J. *et al.* (2002) “Migration of zebrafish spinal motor nerves into the periphery requires multiple myotome-derived cues,” *Developmental Biology*, 252(2), pp. 241–256.

Zeller, J. and Granato, M. (1999) “The zebrafish diwanka gene controls an early step of motor growth cone migration,” *Development (Cambridge, England)*, 126(15), pp. 3461–3472.

Zhang, Y. *et al.* (2014) “An RNA-sequencing transcriptome and splicing database of glia, neurons, and vascular cells of the cerebral cortex,” *The Journal of Neuroscience: The Official Journal of the Society for Neuroscience*, 34(36), pp. 11929–11947. Available at: https://doi.org/10.1523/JNEUROSCI.1860-14.2014.

726

Figure 1.

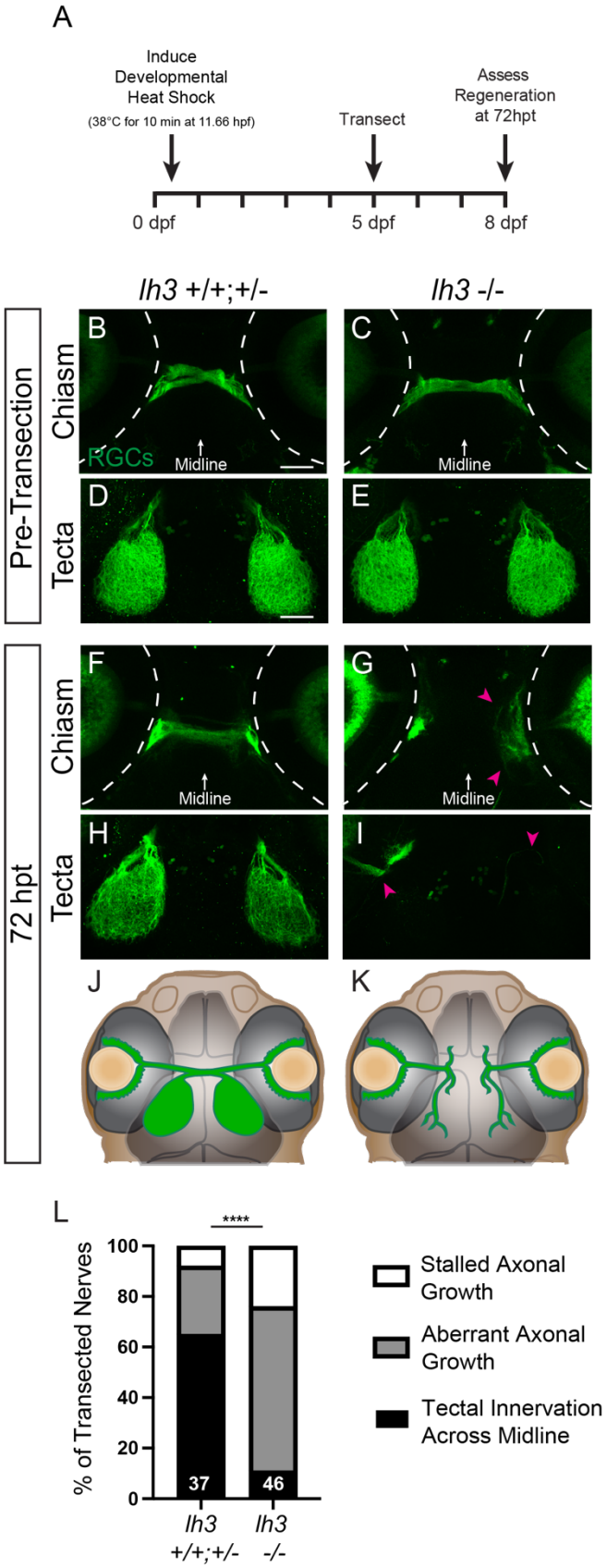

727

728 **Figure 1. Lh3 is required for growth across the midline during regeneration.** (A) Timeline of
729 a transection experiment with *lh3* larvae (hpf, hours post fertilization; dpf, days post fertilization;
730 hpt, hours post transection). (B-C) Before injury, RGC axons labeled by *Tg(isl2b:GFP)* in siblings
731 and conditional *lh3* mutants cross the midline and (D-E) innervate contralateral tecta. (F-I) In
732 contrast to *lh3* siblings at 72 hpt, RGC axons in *lh3* mutants turn away from the midline, project
733 aberrantly (magenta arrowheads) and do not reinnervate contralateral optic tecta. (B-I) Dashed
734 lines indicate the outline of the eyes; scale bars = 50 μm (J-K) Schematics of RGC axonal growth
735 at 72 hpt for (J) *lh3* siblings and (K) *lh3* mutants. (L) Quantification of the percent of nerves at 72
736 hpt that grew across the midline to reinnervate the optic tectum, did not grow across the midline
737 and instead grew along aberrant trajectories or showed stalled axonal growth. Numbers indicate
738 total number of transected nerves. **** $P<0.0001$, Chi squared test. Representative images of
739 chiasms and tecta for each timepoint are of the same fixed larva, though across timepoints are
740 different larvae.
741

742 **Figure 2.**

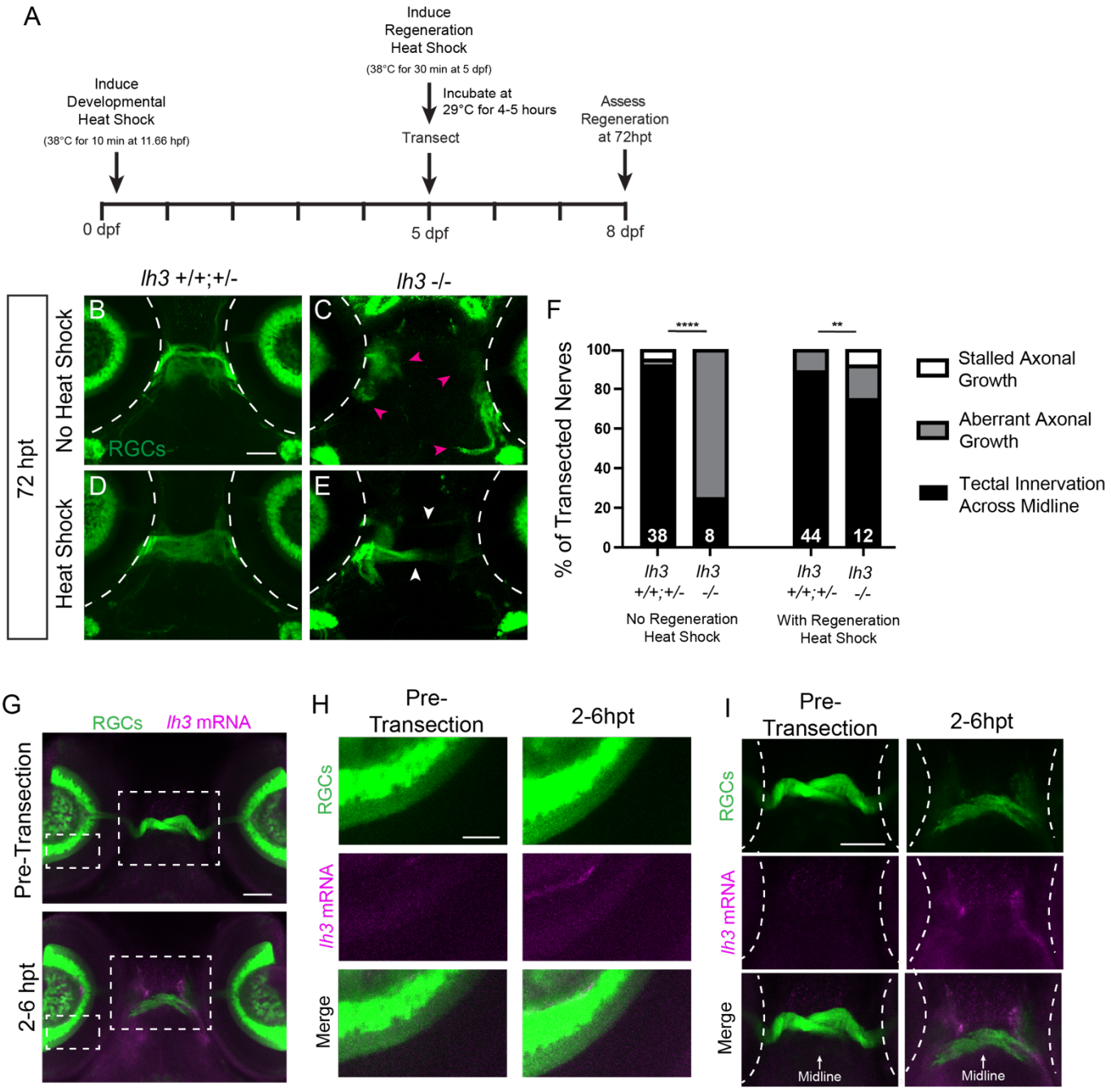

743

744 **Figure 2. *Lh3* expression is upregulated in the optic chiasm during early regeneration.** (A)
745 Timeline of induced Lh3 expression with *Tg(hsp70:lh3-myc)* during development as well as
746 regeneration (hpf, hours post fertilization; dpf, days post fertilization; hpt, hours post transection).
747 (B-C) At 72 hpt in *lh3* siblings with no Heat Shock induction, RGC axons cross the midline to
748 innervate the optic tecta, while RGC axons in *lh3* mutants turn away from the midline and project

749 aberrantly (C, magenta arrowheads). (D-E) In *lh3* siblings and mutants that received a heat shock,
750 RGC axons project across the midline (E, white arrowheads) and innervate the optic tecta.
751 Dashed lines indicate the outline of the eyes; scale bar = 50 μm. (F) Quantification of the percent
752 of nerves at 72 hpt that grew across the midline to reinnervate the optic tectum, did not grow
753 across the midline and instead grew along aberrant trajectories or showed stalled axonal growth
754 in *Tg(isl2b:GFP)* larvae with and without a regeneration heat-shock. Numbers indicate total
755 number of transected nerves. ****$P<0.0001$, **$P<0.01$, chi squared test. (G-I) *Lh3* mRNA
756 expression in *Tg(isl2b:GFP)* larvae pre-transection and at 2-6 hpt. (G) White dashed boxes are
757 areas of the retina shown in (H) and the optic chiasm shown in (I). Scale bars, (G) 50 μm, (H) 20
758 μm, (I) 50 μm. Axons in the chiasm region at 2-6 hpt have not yet fully degenerated following
759 transection. Dashed lines indicate the outline of the eyes in (I). Representative images across
760 timepoints are of different larvae.
761

762 **Figure 3.**

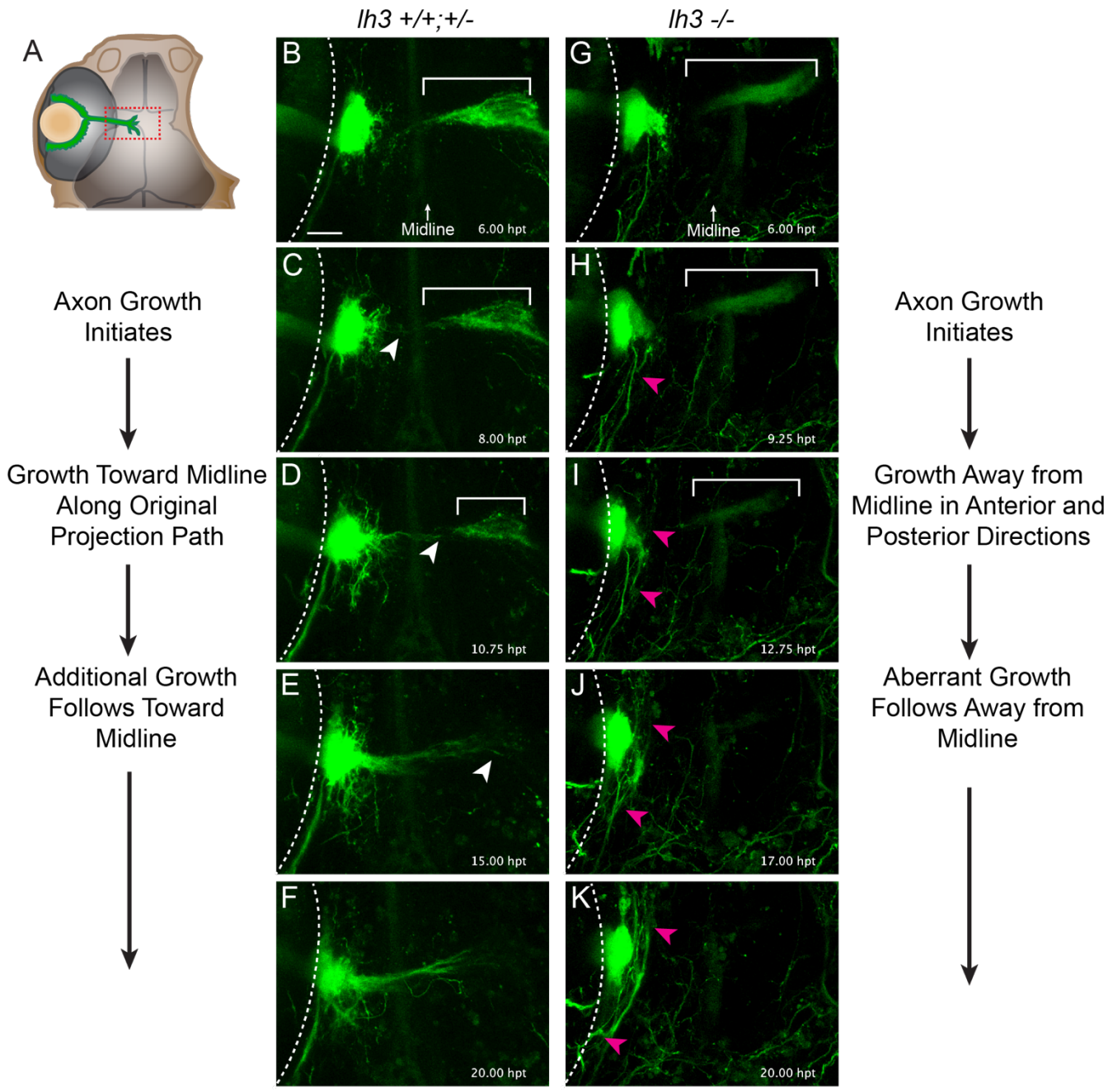

763

764 **Figure 3. *Lh3* directs the initial regrowing RGC axons.** (A) Schematic of larvae expressing
765 *Tg(isl2b:GFP)* to label RGCs that were used for *in vivo* imaging. Larvae have one eye removed
766 one day prior to timelapse imaging. Red box indicates the region imaged in panels B-K. (B,G)
767 Transected RGC axons separate from the distal portion of the optic nerve that will eventually
768 degenerate (indicated by brackets in B-D, G-I). (C) In *lh3* siblings, RGC axons initiate growth out
769 from the proximal stump. (D) A small group of axons (white arrowhead) project directly toward the

770 midline along the original path of the projection and then (E-F) subsequently additional axonal
771 growth follows (n = 7/10 nerves). (H) In *lh3* mutants, axons grow out from the proximal stump, but
772 (I-K) persist along aberrant trajectories (magenta arrowheads; n = 6/12 nerves). See also Figure
773 S1. Dashed lines indicate the outline of the eyes; scale bar = 25 μm.
774

775 **Figure 4.**

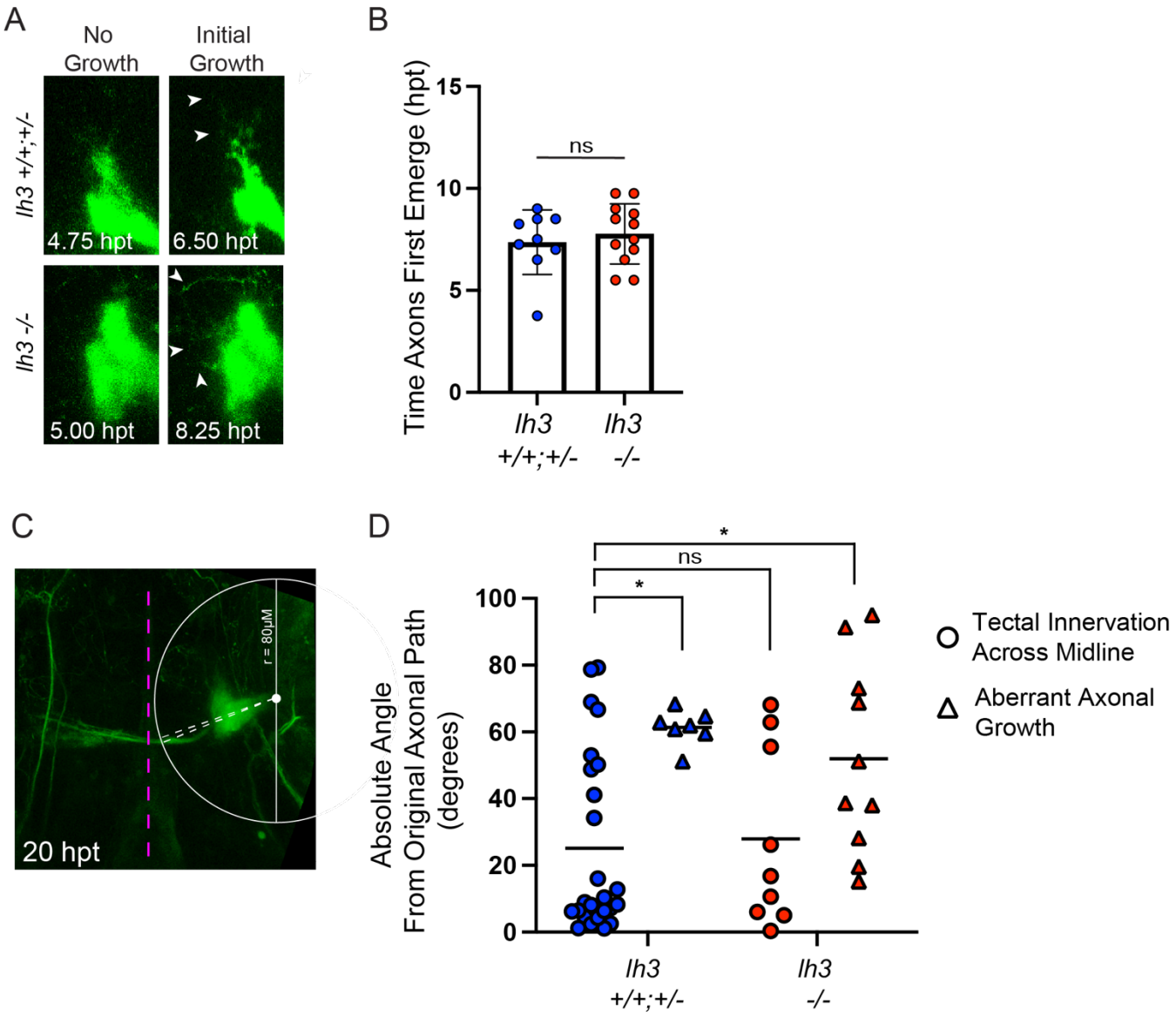

776

777 **Figure 4. *Lh3* is required to direct regrowing RGC axons along their original path.** (A)
778 Representative frames from live timelapses of larvae expressing *Tg(isl2b:GFP)* to label RGCs
779 showing the initial axonal growth that emerges from the injured proximal stump of axons. hpt =
780 hours post transection. (B) Comparison of the time when axon fascicles first emerge from the
781 proximal stump in *lh3* siblings and mutants. Time was determined by the first frame when axon
782 fascicles were observed extending from the proximal stump that extended for at least one other
783 consecutive frame. Data are represented as mean ± SD; n.s.*P>0.05*, t-test. (C) Representative
784 image of a regenerating nerve at 20 hpt and the mark-up to measure the angle of growing fascicles

785 from the injured stump of axons. The magenta line marks the parasphenoid cartilage. See
786 Methods for more details on quantifications. (D) Quantification at 20 hpt of the absolute angle of
787 axon fascicles from the end of a projection to the path of the original axonal projection. (Tectal
788 Innervation Across Midline, sibling n = 6 nerves, mutants n = 3 nerves; Aberrant Axonal Growth,
789 sibling n = 3 nerves, mutants n = 6 nerves). Individual dots are measured fascicle absolute angles,
790 lines represent means; one-way ANOVA, n.s.$P>0.05$, * $P<0.05$. See Supplemental Table 1 for
791 individual angles.
792

Figure 5.

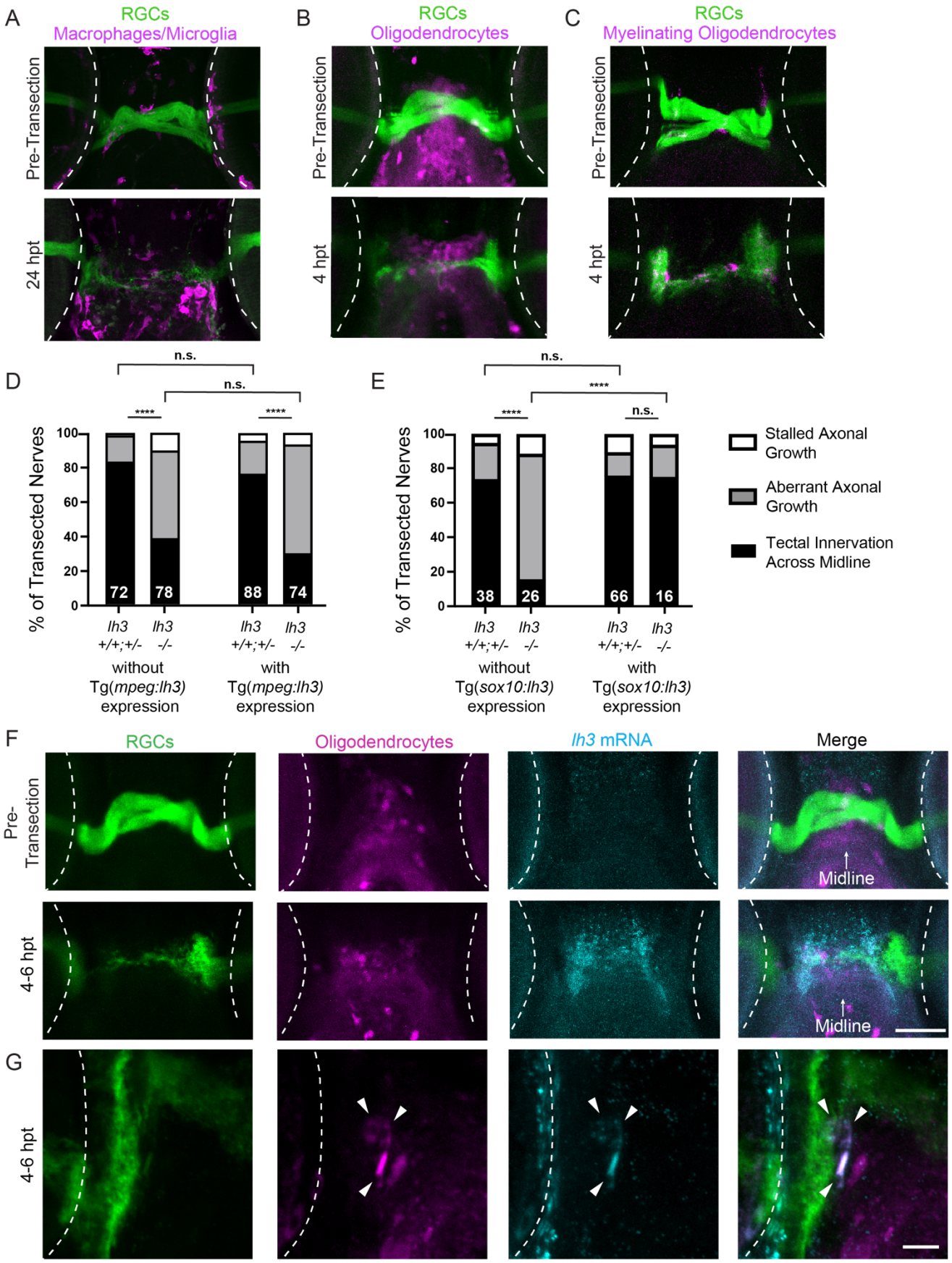
A
RGCs
Macrophages/Microglia
Pre-Transection
24 hpt
B
RGCs
Oligodendrocytes
Pre-Transection
4 hpt
C
RGCs
Myelinating Oligodendrocytes
Pre-Transection
4 hpt
D
n.s.
n.s.
****
****
% of Transected Nerves
100
80
60
40
20
0
72
78
88
74
lh3 +/+;+/-
lh3 -/-
lh3 +/+;+/-
lh3 -/-
without Tg(mpeg:lh3) expression
with Tg(mpeg:lh3) expression
E
n.s.
****
****
n.s.
% of Transected Nerves
38
26
66
16
lh3 +/+;+/-
lh3 -/-
lh3 +/+;+/-
lh3 -/-
without Tg(sox10:lh3) expression
with Tg(sox10:lh3) expression
Stalled Axonal Growth
Aberrant Axonal Growth
Tectal Innervation Across Midline
F
RGCs
Oligodendrocytes
lh3 mRNA
Merge
Pre-Transection
Midline
4-6 hpt
Midline
G
4-6 hpt

795 **Figure 5. Lh3 in *sox10* expressing glia restores RGC axonal growth across the midline.** (A)
796 In wild-type larvae expressing *Tg(isl2b:GFP)* to label RGCs, macrophages and microglia labeled
797 by *Tg*(*mpeg1:Gal4FF*);*Tg*(*UAS:nfsB-mCherry*) are observed in the area of the optic chiasm before
798 transection. At 24 hours post transection (hpt), an influx of *mpeg*+ cells is seen. (B-C)
799 Oligodendrocyte lineage cells labeled by *Tg(olig2:dsred)* as well as *mbpa* mRNA expression in
800 myelinating oligodendrocytes are also seen in the chiasm before and after transection, near the
801 injured proximal stump of RGC axons or along the degenerating original projection. (D)
802 Quantification of the percent of nerves at 72 hpt that grew across the midline to reinnervate the
803 optic tectum, did not grow across the midline and instead grew along aberrant trajectories or
804 showed stalled axonal growth with and without *Tg(mpeg:lh3-myc)* transgene. Numbers indicate
805 total number of transected nerves. ****$P<0.0001$, n.s. $P>0.05$, chi squared test. (E) Quantification
806 of regeneration with and without *Tg(sox10:lh3-mkate)* transgene. Numbers indicate total number
807 of transected nerves. ****$P<0.0001$, n.s. $P>0.05$, chi squared test. (F) *Lh3* mRNA expression at
808 4-6 hpt is upregulated and overlaps with oligodendrocytes labeled by *Tg(olig2:dsred)*. scale bars
809 = 100um (G) Additional images of individual oligodendrocytes labeled by *Tg(olig2:dsred)* co-
810 expressing *lh3* mRNA (see also Supplementary Movie 3). scale bars = 10um. Representative
811 images across timepoints are of different larvae. Axons in the chiasm region at 4-6 hpt have not
812 yet fully degenerated following transection. Dashed lines indicate the outline of the eyes.
813

Figure 6.

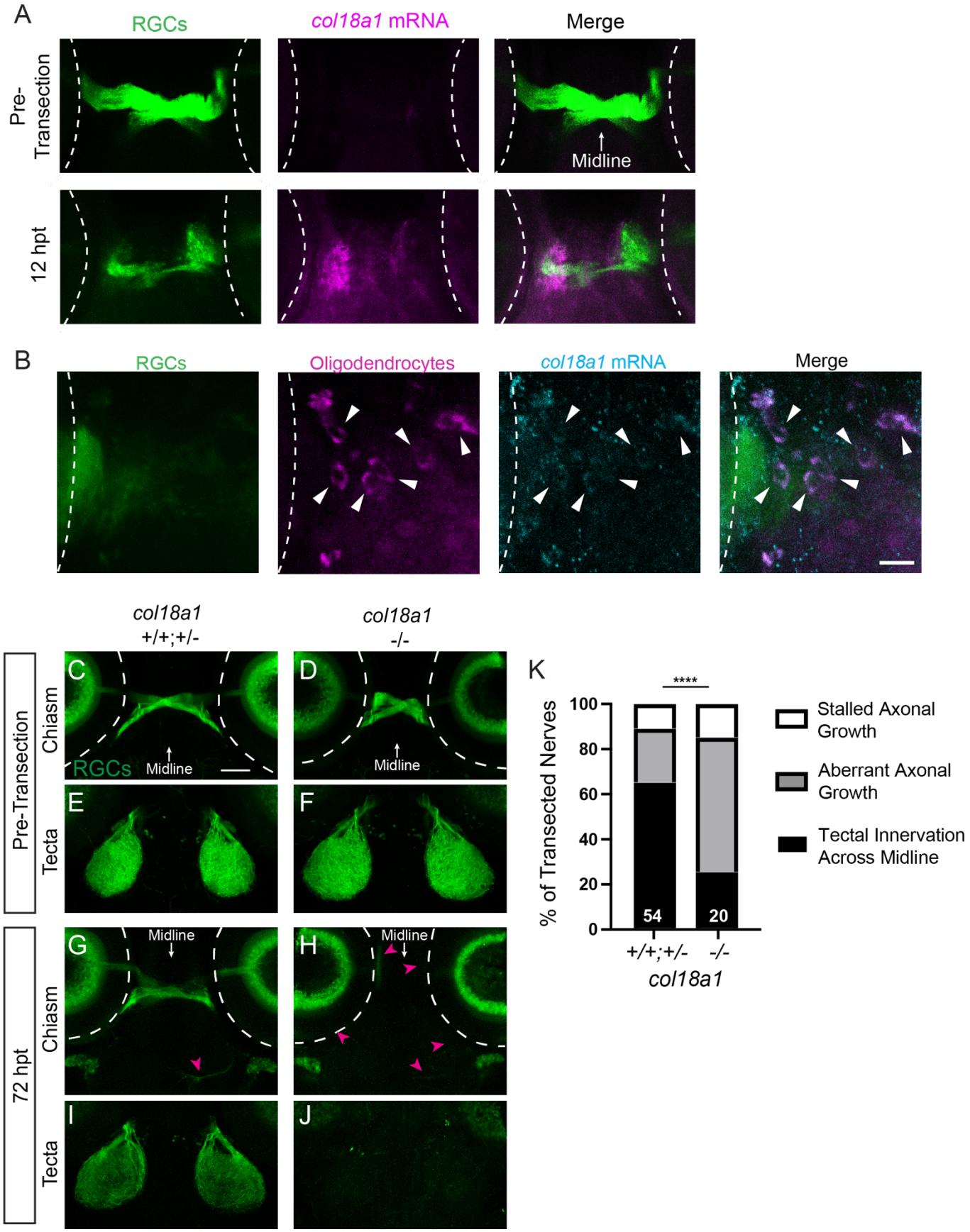
A
RGCs
col18a1 mRNA
Merge
Pre-Transection
12 hpt
Midline
B
RGCs
Oligodendrocytes
col18a1 mRNA
Merge
col18a1 +/+;+/-
col18a1 -/-
Pre-Transection
Chiasm
Tecta
72 hpt
C
D
E
F
G
H
I
J
RGCs
Midline
K
****
% of Transected Nerves
100
80
60
40
20
0
54
20
+/+;+/-
-/-
col18a1
Stalled Axonal Growth
Aberrant Axonal Growth
Tectal Innervation Across Midline

816 **Figure 6. The Lh3 candidate substrate Col18a1 is upregulated after transection and directs**
817 **RGC axons across the midline during regeneration.** (A) *Col18a1* mRNA expression pre-
818 transection and at 12 hours post transection (hpt) in larvae expressing *Tg(isl2b:GFP)* to label
819 RGCs. Axons in the chiasm region at 12 hpt have not yet fully degenerated following transection.
820 (B) Additional images of individual oligodendrocytes labeled by *Tg(olig2:dsred) co-expressing lh3*
821 mRNA (see also Supplementary Movie 4). scale bars = 10um. (C-D) Before injury, RGC axons
822 labeled by *Tg(isl2b:GFP)* in siblings and *col18a1* mutants cross the midline and (E-F) innervate
823 contralateral tecta. (G-J) In contrast to *col18a1* siblings at 72 hpt, RGC axons in *col18a1* mutants
824 turn away from the midline, project aberrantly (magenta arrowheads) and do not reinnervate
825 contralateral optic tecta. Dashed lines indicate the outline of the eyes; scale bar = 50 μm. (K)
826 Quantification of the percent of nerves at 72 hpt that grew across the midline to reinnervate the
827 optic tectum, did not grow across the midline and instead grew along aberrant trajectories or
828 showed stalled axonal growth. Numbers indicate total number of transected nerves. ****$P<0.0001$,
829 chi squared test. Representative images of chiasms and tecta for each timepoint are of the same
830 fixed larva, though across timepoints are different larvae.

831 **Supplemental Figure 1.**

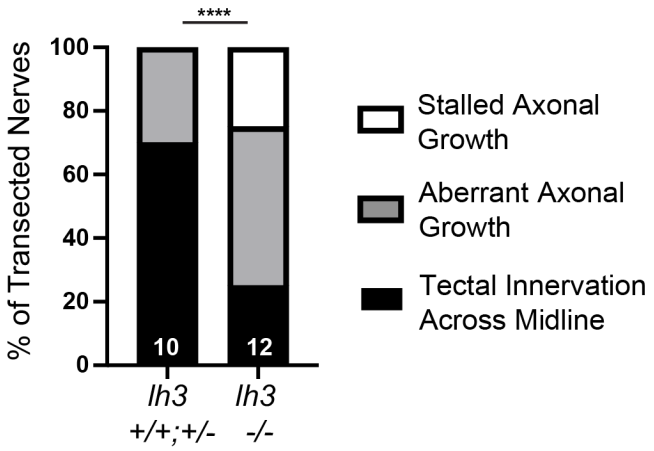

832

833 **S1 Figure. Related to Figures 3 and 4.** Quantification of the percent of nerves from timelapsed

834 larvae that grew across the midline to reinnervate the optic tectum, did not grow across the

835 midline and instead grew along aberrant trajectories, or did not exhibit any axonal growth, ie.

836 stalled, at 72 hpt. Numbers indicate total number of transected nerves. *P<0.00001*, Fisher's

837 exact test.

838 **Supplemental Figure 2.**

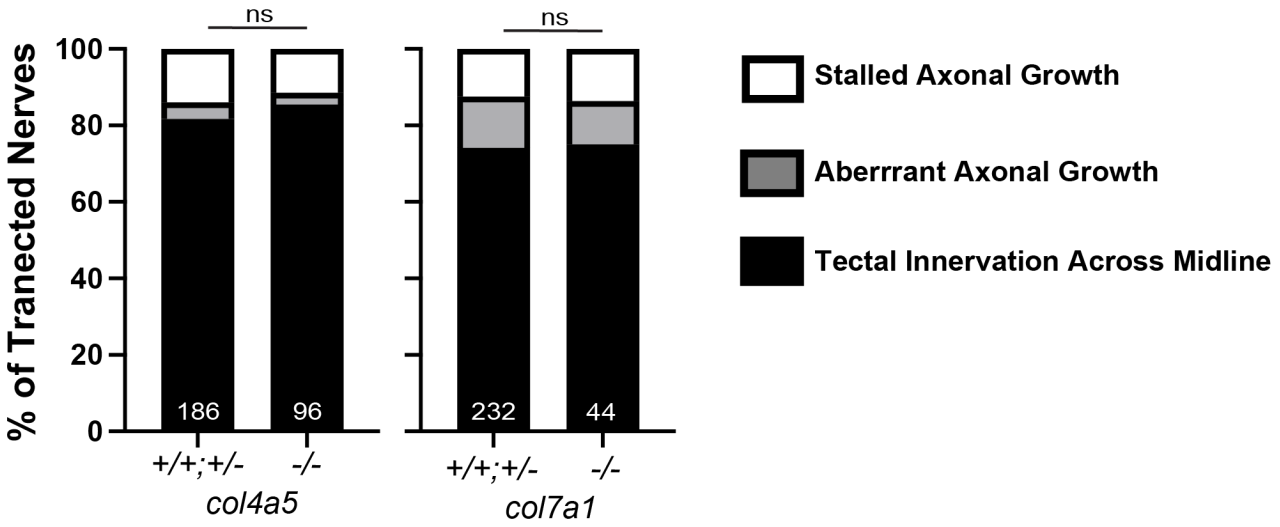

839

840 **S2 Figure. *Col4a5* and *col7a1* are not required to direct regrowing RGC axons to the midline**
841 **during regeneration.** Quantification of the percent of nerves that grew across the midline to
842 reinnervate the optic tectum, did not grow across the midline and instead grew along aberrant
843 trajectories, or did not exhibit any axonal growth, ie. stalled, at 72 hpt. Numbers indicate total
844 number of transected nerves. n.s.$P>0.05$, chi-square test.

845 **Supplemental Information**

846 **Supplementary Movie 1.** Related to Figure 2, contains the movie which corresponds to the *lh3*
847 sibling axonal regeneration time series shown in Figure 2B-F.

848 **Supplementary Movie 2.** Related to Figure 2, contains the movie which corresponds to the *lh3*
849 sibling axonal regeneration time series shown in Figure 2G-K.

850 **Supplementary Movie 3.** Related to Figure 5G, representative three-dimensional rotation from a
851 confocal z-stack demonstrating co-expression of *lh3* mRNA with *Tg(olig2:dsred)*
852 oligodendrocytes.

853 **Supplementary Movie 4.** Related to Figure 6B, representative three-dimensional rotation from a
854 confocal z-stack demonstrating co-expression of *col18a1* mRNA with *Tg(olig2:dsred)*
855 oligodendrocytes.

856

857 **Supplemental Table 1.** Related to Figure 4, contains raw data of individual angles of fascicles
858 from nerves that grew either across the midline or aberrantly from *lh3* sibling and mutant larvae.

859